

Bond properties of steel and sand-coated GFRP bars in Alkali activated cement concrete

Biruk Hailu Tekle*, Yifei Cui and Amar Khennane

School of Engineering and Information Technology, UNSW Canberra, Australia

(Received November 21, 2018, Revised February 7, 2020, Accepted February 10, 2020)

Abstract. The bond performance of glass fibre reinforced polymer (GFRP) bars and that of steel bars embedded in Alkali Activated Cement (AAC) concrete are analysed and compared using pull-out specimens. The bond failure modes, the average bond strength and the free end bond stress-slip curves are used for comparison. Tepfers' concrete ring model is used to further analyse the splitting failure in ribbed steel bar and GFRP bar specimens. The angle the bond forces make with the bar axis was calculated and used for comparing bond behaviour of ribbed steel bar and GFRP bars in AAC concrete. The results showed that bond failure mode plays a significant role in the comparison of the average bond stress of the specimens at failure. In case of pull-out failure mode, specimens with ribbed steel bars showed a higher bond strength while specimens with GFRP bars showed a higher bond stress in case of splitting failure mode. Comparison of the bond stress-slip curves of ribbed steel bars and GFRP bars depicted that the constant bond stress region at the peak is much smaller in case of GFRP bars than ribbed steel bars indicating a basic bond mechanism difference in GFRP and ribbed steel bars.

Keywords: Alkali activated cement (AAC), GFRP bars, bond behaviour, Pull-out failure, Splitting failure, Bond-angle

1. Introduction

Corrosion in steel reinforced concrete structures and the high environmental footprint of the cement industry have led scientists and engineers to look not only for better reinforcement materials but also for alternatives to Ordinary Portland Cement (OPC) concrete. Fibre reinforced polymers (FRP) stand out as ideal alternatives for steel reinforcement while alkali activated cement (AAC) concrete could replace OPC concrete. FRP bars are non-metallic reinforcement. They are manufactured from thermoset polymers vinyl ester and different types of fibres such as glass (GFRP) or carbon fibres (CFRP) and are characterised by high tensile strength, high durability, light weight, and electromagnetic permeability (Bank 2006). AAC concrete can be produced from by-product materials that are rich in silica and alumina, such as fly ash, slag and rice husk ash, mixed with alkali liquids such as metal hydroxide and/or alkali silicate. Unlike OPC concrete, the production of AAC concrete does not depend on calcination of limestone, and hence does not release CO₂ to the atmosphere. In addition to environmental benefits, AAC concrete also provides a rapid rate of strength development, resistance to sulphate attack, acid resistance, little drying shrinkage, low creep, improved resistance to fire, and prolonged handling time (Hardjito and Rangan 2005, Junaid *et al.* 2014, Junaid *et al.* 2015a, Junaid *et al.* 2015b, Neupane *et al.* 2018). Large-scale tests such as beams, columns, pipes, precast bridge decks and beam-

column connections using AAC concrete have also shown the comparable performance of AAC with conventional OPC concrete (Hung Mo *et al.* 2016, Deepa Raj *et al.* 2016). Since these can be classified as novel materials, a study of the reinforcement-to-concrete bond behaviour is warranted. Bond allows forces to be transferred from the surrounding concrete to the reinforcement thus maintaining composite action. Without bond, the reinforcement will slip out of the concrete and become completely ineffective.

It is not surprising therefore, that some research effort has been dedicated to investigating the bond properties of these materials. Benmokrane *et al.* (1996) investigated the bond properties of GFRP and ribbed steel bars embedded in OPC concrete. They observed lower bond strength values of GFRP bars compared to steel bars. This was also reported by Tighiouart *et al.* (1998). In both studies, this difference in bond strength was attributed to the difference of the surface deformations. Bond mechanism mainly depends on adhesion, friction and mechanical bearing. Ribbed steel bars gain most of their bond strength from the mechanical interlock of the concrete and the deformation of the bar. GFRP bars on the other hand, as observed by Benmokrane *et al.* (1996), showed evidence of shearing off of the deformation, implying adhesion and friction dominance. This behaviour was also reported by Pecce *et al.* (2001). However, one thing which should be emphasised here is the type of GFRP bar used. Due to lack of standardization, there are different types of GFRP bars with different geometry and surface conditions, consequently different bond mechanism. Both Benmokrane *et al.* (1996) and Tighiouart *et al.* (1998) used deformed GFRP bars.

Another critical difference between steel and GFRP reinforced OPC concrete was the slip values measured at

*Corresponding author, Ph.D.
E-mail: birukh.tekle@gmail.com

the loaded end and at the free end. The free end slip values for GFRP reinforced OPC concrete are significantly different from the loaded end (Pecce *et al.* 2001, Baena *et al.* 2009, Okelo and Yuan 2005). This is in contrast to steel reinforced OPC concrete specimens where the difference between the two slip values is negligible (Pecce *et al.* 2001, Focacci *et al.* 2000). The low elastic modulus of GFRP bars is the main cause of the slip variation along the embedment length. Thus, the general assumption of constant bond stress distribution along the embedment length cannot be used in case of GFRP bars. This further complicates the assessment of bond slip laws, as there will be two significantly different sets of bond slip curves, for the free end and the loaded end.

Maranan *et al.* (2015) compared the bond performance of steel reinforced AAC concrete and GFRP reinforced AAC concrete specimens. However, their bond-slip curves displayed unusual behaviour. This, as described in Tekle *et al.* (2016), was due to a problem in the experimental setup. Cui and Kayali (2013) investigated the bond performance of steel reinforced AAC concrete. Their results showed that steel reinforced AAC concrete exhibited a better bond strength than the OPC alternative, the reason being the higher splitting tensile strength of AAC concrete. Tekle *et al.* (2016, 2017a, 2017b, 2019) studied the bond performance of GFRP reinforced AAC concrete and compared it with GFRP reinforced OPC concrete. Their results showed the comparable bond performance of GFRP reinforced AAC concrete to that of GFRP reinforced OPC concrete in terms of bond stress-slip relationships, bond distribution and splice length requirements. Despite all these researches, no research has been reported on the bond stress-slip curves of steel reinforced AAC concrete, showing that the bond properties of steel reinforced as well as GFRP reinforced AAC concrete still need further investigations, particularly on issues such as bond stress-slip curves, failure modes and bond strength. The aim of this study therefore is to compare the bond performance of steel reinforced AAC concrete and GFRP reinforced AAC concrete. The comparison will be based on failure modes, bond strength, bond stress-slip curves and analytical bond stress-slip curve parameters. Furthermore, the paper looks in detail into the angle made by the bond stress and the bar axis (bond-angle) in an effort to understand its effect on bond strength and bond failure mode.

2. Experimental results

Bond tests were conducted for both steel and GFRP bars. Pull-out specimens were prepared by embedding GFRP and steel bars in 100 mm diameter x 170 mm high AAC concrete cylinders. In addition to this experimental result, the analysis of this paper is also based on the experimental results from Tekle *et al.* (2016) and Cui and Kayali (2013) which use similar specimens and setting as to the current experiments. Straight (non-deformed) sand-coated GFRP bars with a nominal diameter of 15.9 mm, minimum guaranteed tensile strength of 1184 MPa and elastic modulus of 62.6 GPa were used (Fig. 1 (b)). These were manufactured using a pultrusion process, and are

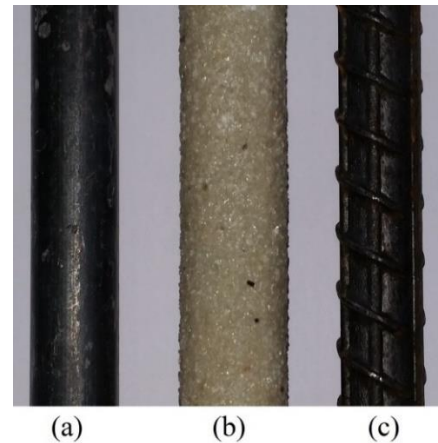


Fig. 1 Reinforcement bars: (a) plain steel bar; (b) sand-coated GFRP bar (c) ribbed steel bar

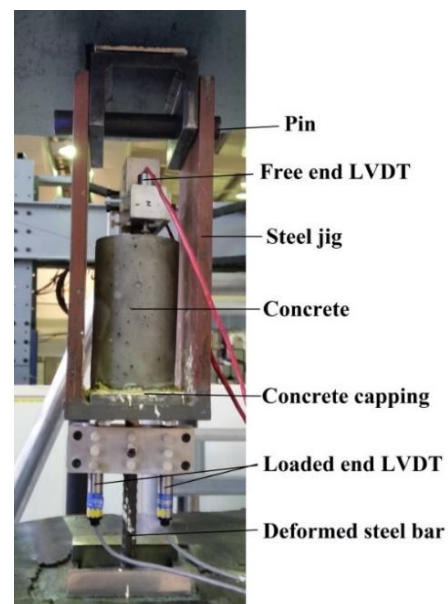


Fig. 2 Typical pull-out experiment setup

produced from continuous E-glass fibres, with a minimum volume of 65 %, bound together by a modified vinyl ester with a maximum volume of 35 %. Normal ductility hot-rolled ribbed steel bars with 16 mm diameter and a yield and ultimate strength values of 546 MPa and 633 MPa respectively were used (Fig. 1 (c)). Plain steel bars with 16 mm diameter and a yield and ultimate strength values of 339 MPa and 507 MPa respectively were also used (Fig. 1 (a)).

The AAC concrete used in all experimental programs is fly ash based. The mix proportions and properties of the concrete are as given in Table 1. The pull-out test setup used for the experiments is as shown in Fig. 2.

The experimental results are summarized in Tables 2 and 3 for steel and GFRP bars, respectively. The average bond stress values in the Tables are calculated by assuming a uniform bond stress distribution along the bar and is defined as the shear force per unit surface area of the bar. This definition of average bond stress is followed throughout the analysis, and is calculated as:

Table 1 Mix proportions and mechanical properties

Ingredient / Property	AAC concrete
Fly Ash (kg/m ³)	420
Coarse aggregate (kg/m ³)	1090
Fine Aggregate (kg/m ³)	630
12M NaOH solution (kg/m ³)	60
Na ₂ SiO ₃ solution (kg/m ³)	150
Water (kg/m ³)	31
Superplasticiser (kg/m ³)	4
Viscosity modifier (kg/m ³)	4
Compressive strength (MPa)	47-50
Splitting tensile strength (MPa)	4.4-4.6

$$\tau = \frac{P_{max}}{\pi d l_b} \quad (1)$$

where τ = average bond stress in MPa; P_{max} is applied maximum pull-out load in N; d is nominal diameter of the bar in mm; and l_b is bonded/embedded length in mm.

3. Analysis and discussion

3.1 Failure modes

As can be noticed in Table 2, splitting failure is the dominant failure mode for the ribbed steel bars even at small embedment lengths; the only exception being the very small embedment length of 32 mm. This failure mode is believed to be the result of the low confinement (concrete cover of 42 mm in this case) and the relatively longer embedment lengths of the reinforcement. Similar failure mode was also observed for the GFRP bars with longer embedment lengths, i.e. 96 mm and 144 mm specimens as reported in Table 3. The splitting failure is caused by the radial component of the bond stress, which generates a hoop stress (Tepfers 1979). When the hoop stress exceeds the tensile strength of the concrete, it results in the splitting of the specimens. Yet, this type of failure was not observed in the plain steel bars (Table 2) despite having similar or longer embedment lengths. This depicts the poor bond between the plain steel bar and the concrete, which, unlike the ribbed steel bars and sand-coated GFRP bars, is not enhanced by the ribs or the sand coating, respectively.

After failure, the GFRP bars in both pull-out and splitting failures showed a thin layer of concrete on their surface with no peeling-off of the sand coating as shown in Fig. 3 and Fig. 4. This is indicative of a good adherence between the surface of GFRP bar and the sand coating. To investigate the failure facies in case of ribbed steel bar's pull-out failure, the RS32 specimens were manually saw cut. Remains of the crushed layer of concrete can be noticed between the ribs of the reinforcement as shown in Fig. 4 (a). However, in the case of splitting failure, the amount of crushed concrete which remained on the bar reduced significantly with only very small amount of concrete at the bottom of the ribs as can be seen in Fig. 4 (c). This can also

Table 2 Summary of ribbed steel bar experimental results

Specimen	Load P_{max} (kN)	Average bond stress τ (MPa)	Free end slip (μ m)	Failure mode
RS32-1	34.0	21.2	953	P
RS32-2	39.6	24.6	1102	P
RS48-1	59.2	24.5	577	S
RS48-2	49.4	20.5	662	S
RS120-1	44.8	7.4	5.98	S
RS120-2	60.2	10.0	7.69	S
RS120-3	53.0	8.8	7.15	S
RS120-4	49.6	8.2	7.08	S
RS120-5	45.6	7.6	8.38	S
RS144-1	65.9	9.1	10	S
RS144-2	72.5	10.0	10	S
RS150-1	75.8	10.0	12.20	S
RS150-2	64.2	8.5	2.5	S
PS120-1	24.8	4.1	1433	P
PS120-2	21.5	3.6	1305	P
PS120-3	28.4	4.7	389	P
PS120-4	24.7	4.1	208	P
PS150-1	20.2	2.7	1664	P
PS150-2	17.2	2.3	-	P
PS150-3	30.0	4.0	1406	P

RS32-1 = Ribbed Steel bar with 32 mm embedment length and specimen number 1

PS120-1 = Plain Steel bar with 120 mm embedment length and specimen number 1

P = Pull-out failure, S = Splitting failure

Table 3 Summary of GFRP bar experimental results (Tekle *et al.*, 2016)

Specimen	Load P_{max} (kN)	Average bond stress τ (MPa)	Free end slip (μ m)	Failure mode
G48-1	45.8	19.0	242	P
G48-2	43.3	18.0	374	P
G48-3	47.2	19.6	355	P
G96-1	89.1	18.5	289	S
G96-2	76.7	15.9	136	S
G96-3	90.7	18.8	182	S
G144-1	109.9	15.2	66	S
G144-2	93.8	12.9	55	S
G144-3	121.9	16.8	64	S

G48-1 = GFRP bar with 48 mm embedment length and specimen number 1.

be observed in Fig. 3 (b), where the concrete interface is intact with little or no damage as the specimen splits. On the other hand, and despite the pull-out failure, the plain steel bar slipped out of the concrete without damaging the interface. As can be seen in Fig. 3 (d), the concrete-plain steel bar interface was intact without damage from the bars.

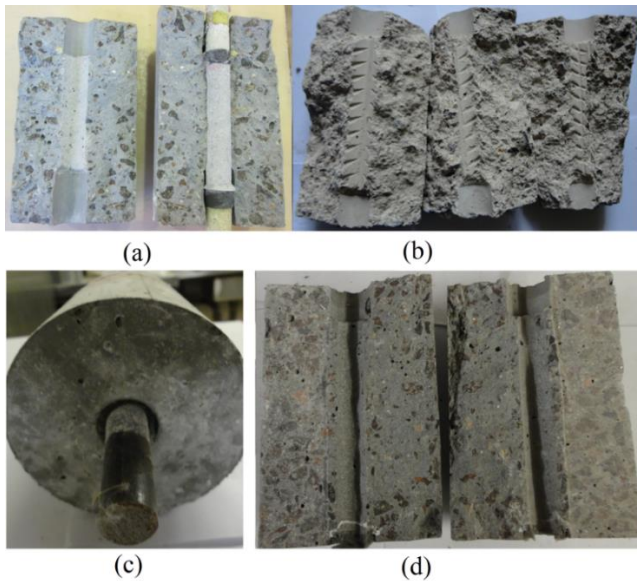


Fig. 3 Bar and concrete surface after failure: (a) G96-1; (b) RS120-1 (c) PS120-1 after pull-out failure; (d) PS120-1 after saw cutting



Fig. 4 Bar surface after failure: (a) RS32-1; (b) G144-1; (c) RS144-1

3.2 Pull-out failure and bond strength

At lower embedment lengths (48 mm for GFRP and 32 mm for ribbed steel bars), failure tend to take place by pull-out. This type of failure is characterised by an interface failure. Ribbed steel bar's pull-out failure was due to the crushing of the concrete between the ribs, whereas, crushing of the concrete over the sand surface caused this failure for sand-coated GFRP bars. The ribbed steel bar specimens offer a better pull-out resistance. This is evidenced by the higher bond strength of the RS32 specimens compared to the G48 specimens. Moreover, despite their splitting failure,

which is known to result in lower bond strength, RS48 specimens showed a higher bond strength than G48 specimens, again showing the higher bond strength of ribbed steel bars. Had the RS48 specimens failed in pull-out, their bond strength will at least be equal to the splitting bond stress observed in Table 2. The higher bond strength of ribbed steel bars was also observed by Maranan *et al.* (2015). They reported that GFRP bar specimens with an embedment length of five times the bar diameter showed a similar pull-out failure mode, but lower bond strength than ribbed steel bar specimens with the same embedment length. For pull-out failure to occur in case of GFRP, the sand coated bar needs to slip over the concrete surface. The sand coating and the concrete between the sand grains provide the interlock between the bar and the concrete. Thus, the bond strength is only as strong as this interface interlock and the confinement provided by the concrete. Once the sand grains or the concrete start shearing off, pull-out will occur. However, in case of ribbed steel bars the pull-out failure occurs only when shear cracks initiate in the concrete keys between ribs as shown in Fig. 4. Since the ribs are much stronger and bigger than the sand coating, the pull-out bond strength of ribbed steel bars is higher than that of sand-coated GFRP bars.

3.3 Splitting failure and bond stress

All the GFRP bar specimens with embedment lengths 96 mm and above failed through splitting failure. Similarly, the ribbed steel bars with embedment lengths 48 mm and above failed by splitting failure. This type of failure can be considered as premature because the bond has not yet attained its maximum value. Due to their ribs, the ribbed steel bars generate a higher splitting stress than the GFRP bar resulting in the splitting of the concrete earlier than the GFRP bar specimens. Indeed, as can be noticed in Table 2 and Table 3, the GFRP reinforced AAC concrete specimens show an apparent higher bond stress than ribbed steel reinforced AAC concrete specimens in case of splitting failure. The average bond stress of the G144 specimens is 15.0 MPa, whereas that of the RS144 is only 9.6 MPa.

4. Splitting failure and bond-angle

The bond stresses between a reinforcing bar and the concrete make an angle α with the bar axis as schematically shown in Fig. 5. This angle mainly depends on the type of reinforcing bar used. The stresses are divided into tangential (τ) and radial (σ_r) components. The radial stress component generates a hoop stress (σ_t) around the concrete covering the reinforcement as shown in Fig. 6 (a).

The splitting of the concrete cover is a common bond failure mode in reinforced concrete structures. The hoop stress generated by the radial component of the bond stress is resisted by the tensile strength of the concrete. Once the tensile strength is exceeded by the hoop stress, splitting failure occurs as shown in Fig. 6 (b). When the bond-angle increases, the radial component of the bond stress increases, and this consequently facilitates the splitting failure mode.

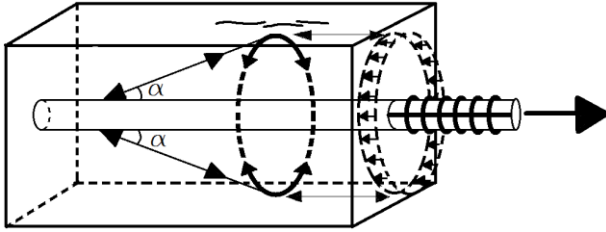


Fig. 5 Radial components of the bond force balanced against tensile stress rings (Tepfers 1979)

Table 4 Average bond-angles

Specimen	Bond stress (MPa)	Tensile strength (MPa)	Uncracked elastic (°)	Partly cracked elastic (°)	Uncracked plastic (°)
G144-1	15.2	4.61	16	30	58
G144-2	12.9	4.61	19	34	62
G144-3	16.8	4.61	15	27	55
Average			17	30	58
RS144-1	9.1	4.42	25	42	69
RS144-2	10.0	4.42	23	40	67
Average			24	41	68

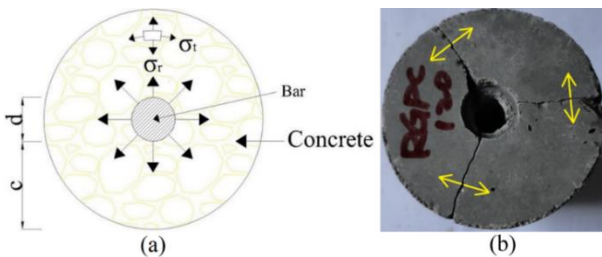


Fig. 6 Splitting failure of ribbed steel bar specimens: (a) Radial and tangential stresses (b) RS120-1 splitting failure

The splitting force depends mainly on the concrete cover thickness, bar diameter and type of bar. As can be seen in Tables 2 and 3, both the deformed steel bars and the GFRP bars have specimens with splitting failure. However, despite the similar cover and bar diameter of these bars, the splitting bond forces are different. Specimens with GFRP bars showed a much higher failure load than those with deformed steel bars. For example, G144 specimens showed an average failure load of 108.5 kN whereas RS144 showed only 69.2 kN. The higher radial bond force generated by the ribbed steel bar caused this early failure of the specimen.

Tepfers (1979) analysed the state of stress in concrete due to bond forces from ribbed reinforcing bars. The radial stresses from the bond were regarded as a hydraulic pressure on the concrete wall. The concrete was modelled in three different ways; uncracked elastic, partly cracked elastic and uncracked plastic. The derived equations for each of these models are as described below:

$$\sigma_t = \tau \tan \alpha \frac{(c + d/2)^2 + (d/2)^2}{(c + d/2)^2 - (d/2)^2} \quad (2)$$

$$\sigma_t = \frac{1.664d\tau \tan \alpha}{(c + d/2)} \quad (3)$$

$$\sigma_t = \frac{d}{2c} \tau \tan \alpha \quad (4)$$

where σ_t is tangential stress, d is diameter of the bar, c is the smallest concrete cover, τ is the bond stress and α is the angle the bond stress makes with the axis of the bar.

Failure of the specimen occurs when the tangential stress equals the tensile strength of the concrete. For comparison purpose, the bond angle is calculated by substituting all the known parameters into Eqs. (2) - (4). Two different sets of specimens with splitting failure, G144 and RS144, were selected for this analysis. The tensile strength of the concrete, is taken as the tangential stress (σ_t). Table 4 summarises these results.

For specimens with an approximate cover to diameter ratio of two, Tepfers recommend using the average of partly cracked elastic and uncracked plastic models (Tepfers 1979). For GFRP bars, the bond-angle according to this recommendation becomes 44° , whereas that of ribbed steel bars becomes 54° . Thus, the GFRP bars resulted in a lower bond-angle when compared to the ribbed steel bars. This is logical because the ribbed steel bars have a deformation on their surface whereas the GFRP bars are only sand coated without surface deformation. Tepfers and Lorenzis (2003) also reported the smaller bond angle for sand-coated GFRP bars when compared to ribbed steel bars. As a probable reason for the lower bond-angle, they suggested that, the sanded surface of the bar creates a softening layer with some ability to transfer tension in concrete close to the bar.

The bond-angle plays a significant role in the failure mode of the specimens. The splitting tendency of a reinforcing bar increases with increasing of the bond-angle (Tepfers and Olsson 1992). Tepfers (1979) calculated the radial component of the bond stress as per Eq. (5). As per this equation for a bond stress of 9.6 MPa, which is the average maximum bond stress obtained for ribbed steel bar specimens (RS144), a radial stress of 13.2 MPa is generated and this was capable of splitting the AAC concrete.

$$\sigma_r = \tau \tan \alpha \quad (5)$$

At the same bond stress level of 9.6 MPa, the GFRP bars (which have a bond-angle of 44° instead of 54°) generated a radial stress of only 9.3 MPa and this was not sufficient to split the AAC concrete. This explains why the specimens with ribbed steel bars failed earlier than their GFRP counterparts in case of splitting failure.

5. Bond stress-slip curves

Bond behaviour is presented in terms of bond stress-slip curves. These are plots of the bond stress and the slip between the reinforcement and the concrete. They show the bond stress - slip pattern at different load levels, the maximum bond stress and the slip at the maximum bond stress. The average bond stress is calculated by assuming a uniform bond stress distribution along the bonded length of the reinforcing bar as per Eq. (1), whereas the slip is defined as the relative displacement between the bar and the concrete. Bond stress-slip curves are regarded as a standard way of representing bond behaviour between concrete and

steel, and are used extensively (Girard and Bastien, 2002, Hong and Park, 2012). Tang 2015 divides the bond stress-slip curve into five phases i.e. non-slip, slight slip, splitting, decreasing bond stress and residual bond stress phases. The non-slip phases or the high initial stiffness is due to the virgin undisturbed chemical bond between the concrete and the bar. As the load increases and reaches about 30% of the bond strength the chemical bond between bar and concrete fails (Tang 2015). The stiffness gradually decreases due to crack formation in the concrete at the vicinity of the reinforcement. Further increase of the load results in either longitudinal splitting or pull-out failure modes based on the concrete confinement provided. After pull-out failure, the slip increases quickly as the bond stress decreases. The residual phase is a constant bond stress phase with increasing slip. At this phase only frictional force between the bar and the surrounding concrete provides the bond stress.

Both GFRP reinforced AAC concrete and steel reinforced AAC concrete displayed the basic characteristic of a bond stress-slip curve. For low values of bond stress, no significant slip was observed. As the bond stress increases, the slip increases resulting in a lower slope of the curve and gradual failing in either pull-out or splitting. Despite these general similarities, they show significant differences in the value of the maximum bond stress, the slip at that bond stress and the slope of the bond stress-slip curves.

For the cases of splitting failure, the bond stress-slip curve can be divided into two parts: the linear region and the nonlinear region. In addition to these regions, a softening branch is found in case of pull-out failure. Fig. 7 shows different bond stress-slip curves for GFRP, ribbed and plain steel bar specimens. In case of long embedment lengths, the GFRP bar specimens displayed a longer nonlinear region compared to similar embedment length deformed steel bars. This is due to the much brittle failure of the specimens with ribbed steel bars. The small amount of slip observed at the free end of ribbed steel bar specimens further portrays their sudden brittle failure. The average slip recorded for RS120 specimens for instance is only 7 microns, which shows a negligible amount of bar displacement at the free end when the concrete splits. Contrary to the ribbed bars, the plain steel bar specimens displayed a longer nonlinear curve compared to the GFRP bar specimens. This can be attributed to the sand coating of GFRP, which in terms of initiating splitting failure puts GFRP bars between plain and ribbed steel bars.

Further investigation of the relationship between bond stress and slip is performed by comparing the bond stress at different values of free end slips. ACI 440.3R (2012) uses the bond stress values at slips of 0.05, 0.1 and 0.25 mm for such comparison. At all these slips, specimens with GFRP bar recorded a much higher bond stress than those with plain steel bars. G144 specimens for instance, have an average bond stress of 15.3 MPa at 0.10 mm while PS150 specimens showed an average bond stress of only 2.6 MPa at this slip value. Ribbed steel bars on the contrary, displayed a different pattern at different slips. At 0.05 mm and 0.10 mm they displayed a lower bond stress than GFRP

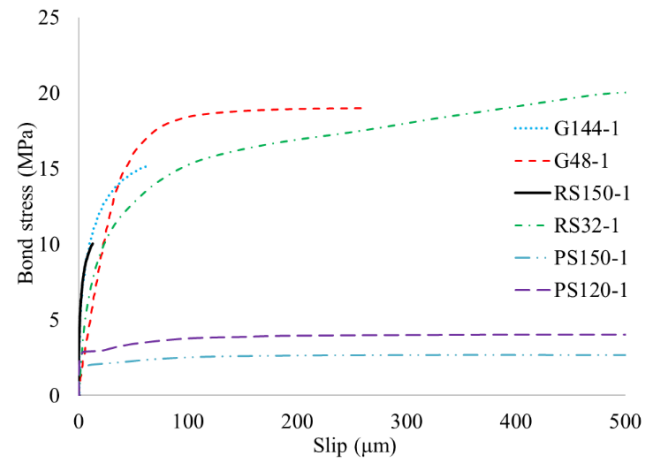


Fig. 7 Bond stress-slip curves for GFRP, ribbed steel and plain steel bars

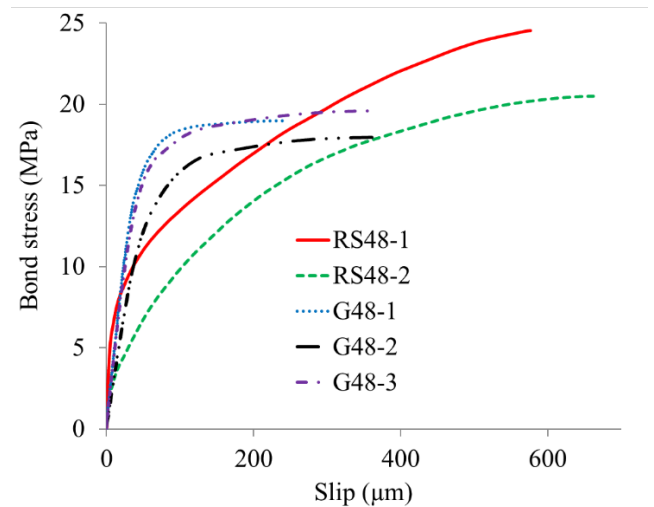


Fig. 8 RS48 and G48 specimens' bond-slip curve

bars. However, at a slip of 0.25 mm the two bond stresses balanced, i.e. both ribbed steel bar and GFRP bar displayed an average bond stress of about 18 MPa as can be observed from Fig. 8. At a higher slip, the GFRP bar specimens recorded a lower bond stress. This is probably due to the initiation of crushing of the concrete on the sand coatings of the GFRP bar which results in higher slippage. In Fig. 8, it can be observed that the ribbed steel bar specimen passes the GFRP bar after a slip of about 250 μm .

At the same slip values, change in embedment length affected the bond stress. For instance, the PS120 specimens recorded an average bond stress of 3.6 MPa at 0.05 mm slip while the PS150 specimens resulted in an average bond stress of 2.43 MPa at the same slip value. This reduction in bond stress is due to the decrease of bond strength with the increase of embedment length. Similarly, the G96 specimens resulted in an average bond stress of 15.3 MPa at 0.05 mm slip whereas the G144 specimens showed a slightly lower bond stress of 14.2 MPa at the same slip value. Both GFRP and plain steel bars' bond stress is affected by the change in embedment length, however, the effect is more pronounced in plain steel bars than GFRP bars.

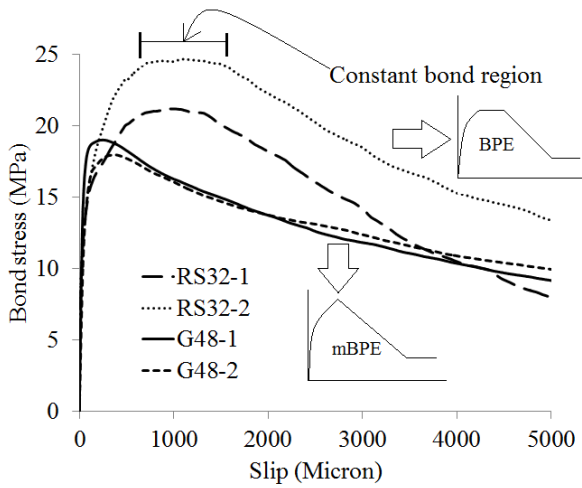


Fig. 9 RS32 and G48 bond-slip curves

The complete bond stress-slip relationships for ribbed steel and GFRP bars are shown in Fig. 9 in the case of pull-out failure. The RS32 displayed a longer nonlinear stage with a region of constant bond stress around the maximum bond stress value. The GFRP bar specimens on the other hand, showed a relatively shorter constant bond region. In fact, Cosezna *et al.* (1997) reported that OPC concrete specimens with FRP bars do not have this constant bond region, and thus devised a new bond-slip model called mBEP by modifying the Eligehausen, Popov, and Bertero model or BEP model developed by Eligehausen *et al.* (1983).

6. Analytical models for bond stress-slip relationship

Analytical models of bond stress-slip relationship are required in advanced numerical modelling of reinforced concrete structures. Different analytical models have been developed to represent the constitutive bond stress-slip relationship of steel and GFRP bars. Some of the most common models are Malvar model, Bertero-Eligehausen-Popov (BEP) model, modified BEP (mBEP) model, and Cosenza-Manfredi-Realfonzo (CMR) model. CMR model describes only the ascending branch; however, in this range shows the best performances and seems very promising in modelling of bond at the serviceability state level (Cosenza *et al.* 1995). This model is as expressed in Eq. (6).

$$\tau(s) = \tau_m \cdot \left(1 - e^{-\frac{s}{s_r}}\right)^\beta \quad (6)$$

where τ_m = maximum bond strength (MPa); s = slip (mm); s_r and β = curve fitting parameters.

The CMR bond stress-slip model parameters were determined for the plain and ribbed steel bars with pull-out failure mode by using curve fitting. These parameters were then compared with GFRP bars' parameters obtained from Tekle *et al.* (2016) which were obtained by taking into account the slip distribution along the embedment length. The parameters were also compared with the parameters from Maranan *et al.* (2015). The results are as presented in Table 5.

Table 5 CMR model parameters

Specimen	CMR parameters		
	τ_m (MPa)	s_r (mm)	β
Ribbed steel bar	22.9	0.20	0.43
Plain steel bar	3.9	0.19	0.10
GFRP (Tekle <i>et al.</i> (2016))	17.6	0.03	1.23
GFRP (Maranan <i>et al.</i> 2015)	21.5	0.14	5

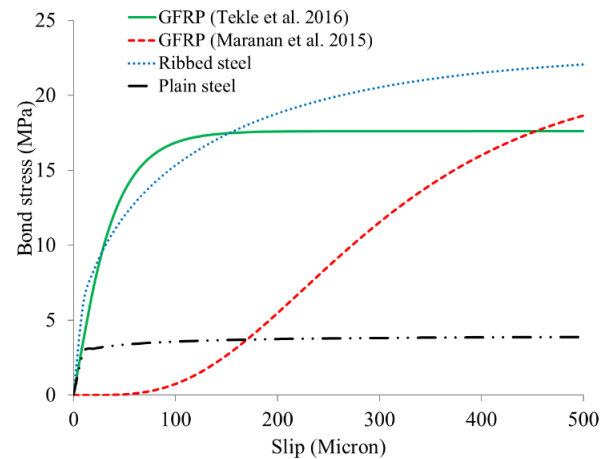


Fig. 10 CMR model bond stress-slip relationship

As can be seen in Table 5, there is a significant difference between the bond stress-slip curve parameters for plain steel bars and GFRP bars. The parameters control the slope of the bond stress-slip curve. Specifically, the s_r mainly controls the slope of the linear part of the curves while β values control the slope of the nonlinear part of the curve. Analytical models with an initial tangent of infinity reproduce the physical phenomenon quite well because experimental tests show that for low value of bond stress no slip are observed due to adhesion (Cosenza *et al.* 1995). As can be seen in Fig. 10, the analytical model developed by Maranan *et al.* (2015) for GFRP bars showed an additional nonlinear region at the start of the curve with an initial tangent of zero contrary to the other curves. As can be seen in Table 5, this model showed the highest β value which resulted in this behaviour. As explained in the introduction, this is due to the experimental setup problems thus should not be used for numerical modelling purpose as it does not simulate the physical phenomenon properly.

Compared to the GFRP bars, the ribbed steel bars displayed a lower value of β and a higher value of s_r . As can be seen in Fig. 10, ribbed steel bars have a higher initial slope and a longer nonlinear region compared to GFRP bars.

Bond in structures can be modelled by either considering a perfect bond between concrete and reinforcement or by using bond stress-slip relationships. Perfect bond or full adherence method is the most common method due to its simplicity (Demir and Husen, 2015). However, it is not an accurate method because of the simplifications involved especially in structures subjected to high stress. Fallah *et al.*, 2013 observed significant

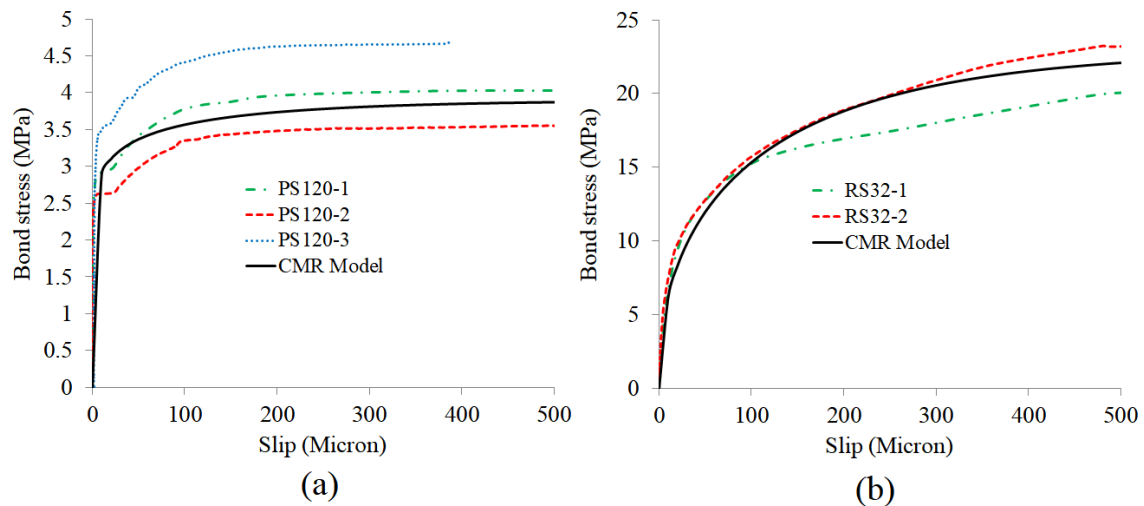


Fig. 11 Experimental and CMR model bond stress-slip: (a) Plain steel bar; (b) Ribbed steel bar

differences in displacements, drifts and other structural behaviors when a structure is modelled with and without bond stress-slip curves. It is therefore important to incorporate the bond stress-slip curves into the modelling to obtain an accurate model. Fig. 11 shows the experimental and the CMR model bond stress-slip relationships. The CMR bond stress-slip model shows a good agreement with the experimental bond stress-slip curves in both the linear and nonlinear region of the bond stress-slip curve. Thus, these models can be used in numerical analysis of reinforced AAC concrete members to simulate the bond stress slip behaviour accurately.

Despite being developed from specimens with pull-out failure, the bond stress-slip model can also be used to simulate specimens with concrete splitting failure mode. In such cases mainly the linear range of the bond stress-slip curves will be utilised by the model as the concrete splits before the bond stress reaches the peak stress value.

7. Conclusions

This paper presented a comparison between the bond properties of plain/ribbed steel bars and sand-coated GFRP bars in AAC concrete. Experimental and analytical results are used for the investigation of different bond behaviours. The following conclusions are made based on the findings of this study:

- Comparison of maximum bond stress of GFRP and ribbed steel bar depends on the type of bond failure mode observed. In case of pull-out failure mode, specimens with ribbed steel bars showed a higher bond strength while specimens with GFRP bars showed a higher bond stress in case of splitting failure mode. This shows the ribbed steel bar's better bond performance and higher splitting tendency.
- Comparison of the bond stress-slip curves of ribbed steel bars and GFRP bars showed that, the constant bond stress region at the peak is much smaller in case of GFRP bars than ribbed steel bars depicting a basic bond mechanism difference.

- Both ribbed steel bars and sand-coated GFRP bars failure modes were dependant on the embedment length of the bar. Lower embedment lengths resulted in pull-out failure, whereas higher embedment lengths resulted in splitting failure.

- Ribbed steel bar's pull-out failure was due to the crushing of the concrete between the ribs, whereas, crushing of the concrete over the sand surface caused this failure for sand-coated GFRP bars.

- Bond-angles of 54° and 44° were determined for ribbed steel bars and sand-coated GFRP bars, respectively. This explains the higher splitting tendency of ribbed steel bars.

Acknowledgement

The scholarship support to the first author from UNSW Canberra is greatly acknowledged.

References

- ACI 440.3R (2012), "Guide Test Methods for Fiber-Reinforced Polymers (FRPs) for Reinforcing or Strengthening Concrete Structures", Michigan, USA.
- Baena, M., Torre L., Turo, A. and Barris, C. (2009), "Experimental study of bond behaviour between concrete and FRP bars using a pull-out test", *Compos. Part B Eng.*, **40**(8), 784-797. <https://doi.org/10.1016/j.compositesb.2009.07.003>.
- Bank, L.C. (2006), *Composites for Construction: Structural Design with FRP Materials*, John Wiley and Sons, Inc., Hoboken, New Jersey, USA.
- Benmokrane, B., Tighiouart, B. and Chaallal, O. (1996), "Bond strength and load distribution of composite GFRP reinforcing bars in concrete", *ACI Mater. J.*, **93**(3), 246-252.
- Cosenza, E., Manfredi, G. and Realfonzo, R. (1995), "Analytical modelling of bond between FRP reinforcing bars and concrete", *Second International RILEM Symposium (FRPRCS-2)*, Ghent, Belgium.
- Cosezna, E., Manfredi, G. and Realfonzo, R. (1997), "Behaviour and Modelling of Bond of FRP Rebars to Concrete", *J. Compos. Construct.*, **1**(2), 40-51.

- 0268(1997)1:2(40).
- Cui, Y. and Kayali, O. (2013), "Bond Performance of Steel Bar and Fly Ash based Geopolymer Concrete", *26th Biennial Conference of the Concrete Institute of Australia: Understanding Concrete*, North Sydney, Australia.
- Deepa Raj, S., Ganesan, N., Abraham, R. and Raju, A. (2016), "Behavior of geopolymer and conventional concrete beam column joints under reverse cyclic loading", *Adv. Concrete Construct.*, **4**(3), 161-172. <http://dx.doi.org/10.12989/acc.2016.4.3.161>.
- Demir, S., Husem, M. (2015), "Investigation of bond-slip modeling methods used in FE analysis of RC members", *Struct. Eng. Mech.*, **56**(2), 275-291. <https://doi.org/10.12989/sem.2015.56.2.275>.
- Eligehausen, R., Popov, E.P. and Bertero, V.V. (1983), "Local bond stress-slip relationships of deformed bars under generalized excitations: Experimental results and analytical model", University of California, Earthquake Engineering Research Centre, Berkeley, USA.
- Fallah, M.M., Shooshtari, A., and Ronagh H.R. (2013), "Investigating the effect of bond slip on the seismic response of RC structures", *Struct. Eng. Mech.*, **46**(5), 695-711. <http://dx.doi.org/10.12989/sem.2013.46.5.695>.
- Focacci, F., Nanni, A. and Bakis, C.E. (2000), "Local bond-slip relationship for FRP reinforcement in concrete", *J. Compos. Construct.*, **4**(1), 25-31. [https://doi.org/10.1061/\(ASCE\)10900268\(2000\)4:1\(24\)](https://doi.org/10.1061/(ASCE)10900268(2000)4:1(24)).
- Girard, C. and Bastien, J. (2002), "Finite-element bond-slip model for concrete columns under cyclic loads", *J. Struct. Eng.*, **128**(12), 1502-1510. [https://doi.org/10.1061/\(ASCE\)07339445\(2002\)128:12\(1502\)](https://doi.org/10.1061/(ASCE)07339445(2002)128:12(1502)).
- Hardjito, D. and Rangan, B.V. (2005), "Development and Properties of Low Calcium Fly Ash-Based Geopolymer Concrete", *Research Report GC 1*, Curtin University of Technology, Perth, Australia
- Hong, S. and Park, S.-K. (2012), "Uniaxial Bond Stress-Slip Relationship of Reinforcing Bars in Concrete" *Adv. Mater. Sci. Eng.*, **2012**, 1-12. <https://doi.org/10.1155/2012/328570>.
- Hung Mo, K., Johnson Alengaram, U., Jumaat, M. Z. (2016), "Structural performance of reinforced geopolymer concrete members: A review", *Construct. Build. Mater.*, **120**(2016), 125-264. <https://doi.org/10.1016/j.conbuildmat.2016.05.088>.
- Junaid, M.T., Kayali, O., Khennane, A. and Black, J., (2015b), "A mix design procedure for low calcium alkali activated fly ash-based concretes" *Construct. Building Mater.*, **79**, 301-310. <https://doi.org/10.1016/j.conbuildmat.2015.01.048>.
- Junaid, M.T., Kayali, O., Khennane, A. (2015a), "Performance of fly ash based geopolymer concrete made using non-pelletized fly ash aggregates after exposure to high temperature", *Mater. Struct.*, **48**(10), 3357-65. <https://doi.org/10.1617/s11527-0140404-6>.
- Junaid, M.T., Khennane, A., Kayali, O., Sadaoui, A., Picard, D., and Fafard M. (2014), "Aspects of the deformational behaviour of alkali activated fly ash concrete at elevated temperatures", *Cement Concrete Res.*, **60**, 24-29. <https://doi.org/10.1016/j.cemconres.2014.01.026>.
- Maranan, G., Manalo, A., Karunasena, K. and Benmokrane, B. (2015), "Bond Stress-Slip Behaviour: Case of GFRP Bars in Geopolymer Concrete", *J. Mater. Civil Eng.*, **27**(1), 1-9. [https://doi.org/10.1061/\(ASCE\)MT.1943-5533.0001046](https://doi.org/10.1061/(ASCE)MT.1943-5533.0001046).
- Neupane, K., Chalmers D., and Kidd, P. (2018), "High-strength Geopolymer Concrete – Properties, Advantages and Challenges" *Adv. Mater.*, **7**(2), 15-25. <https://doi.org/10.11648/j.am.20180702.11>.
- Okelo, R. and Yuan, R.L. (2005), "Strength of fibre reinforced polymer rebars in normal strength concrete" *J. Compos. Construct.*, **9**(3), 203-213. [https://doi.org/10.1061/\(ASCE\)1090-0268\(2005\)9:3\(203\)](https://doi.org/10.1061/(ASCE)1090-0268(2005)9:3(203)).
- Pecce, M., Manfredi, G., Realfonzo, R., and Cosenza, E. (2001), "Experimental and Analytical Evaluation of Bond Properties of GFRP Bars", *J. Mater. Civil Eng.*, **13**(4), 282-290. [https://doi.org/10.1061/\(ASCE\)0899-1561\(2001\)13:4\(282\)](https://doi.org/10.1061/(ASCE)0899-1561(2001)13:4(282)).
- Tang, CW. (2015), "Local bond stress-slip behavior of reinforcing bars embedded in lightweight aggregate concrete", *Comput. Concrete*, **16**(3), 449-466. <https://doi.org/10.12989/cac.2015.16.3.449>.
- Tekle, B.H., Khennane, A. and Kayali, O. (2016), "Bond properties of sand-coated GFRP bars with fly ash based geopolymer concrete", *J. Compos. Construct.*, **20**(5). [https://doi.org/10.1061/\(ASCE\)CC.1943-5614.0000685](https://doi.org/10.1061/(ASCE)CC.1943-5614.0000685).
- Tekle, B.H., Khennane, A. and Kayali, O. (2017a), "Bond behaviour of GFRP reinforcement in alkali activated cement concrete", *Construct. Build. Mater.*, **154**, 972-982. <https://doi.org/10.1016/j.conbuildmat.2017.08.029>.
- Tekle, B.H., Khennane, A. and Kayali, O. (2017b), "Bond of spliced GFRP reinforcement bars in alkali activated cement concrete", *Eng. Struct.*, **147**, 740-751. <https://doi.org/10.1016/j.engstruct.2017.06.040>.
- Tekle, B.H. and Khennane, A. (2019), "Parametric study on bond of GFRP bars in alkali-activated cement concrete", *Mag. Concrete Res.*, <https://doi.org/10.1680/jmacr.18.00364>.
- Tepfers, R. and Lorenzis, L.D. (2003), "Bond of FRP reinforcement in concrete- a challenge", *Mech. Compos. Mater.*, **39**(4), 315-328. <https://link.springer.com/article/10.1023/A:1025642411103>.
- Tepfers, R. and Olsson P-Å. (1992), "Ring test for evaluation of bond properties of reinforcing bars", Riga, Latvia.
- Tepfers, R. (1979), "Cracking of concrete Cover along anchored deformed reinforcing bars", *Mag. Concrete Res.*, **31**(106). <https://doi.org/10.1680/mac.1979.31.106.3>.
- Tighiouart, B., Benmokrane, B. and Gao, D. (1998), "Investigation of bond in concrete member with fibre reinforced polymer (FRP) bars", *Construct. Build. Mater.*, **12**, 453-462. [https://doi.org/10.1016/S0950-0618\(98\)00027-0](https://doi.org/10.1016/S0950-0618(98)00027-0).

PL